Domain-wall dynamics in aligned bound Sm_2Fe_{17}

D.-X. Chen
Instituto de Magnetismo Aplicado, RENFE-UCM, 28230 Las Rozas, Madrid, Spain

V. Skumryev* and J. M. D. Coey
Department of Pure and Applied Physics, Trinity College, Dublin 2, Ireland
(Received 2 January 1996)

ac susceptibility ($\chi_{ac}=\chi'-j\chi''$) of an aligned bound Sm_2Fe_{17} powder sample has been measured along the easy direction as a function of temperature, frequency, warming rate, and time. Anomalous behavior has been found in that with increasing temperature, χ' and χ'' increase steadily up to $T\sim150$ K where a drop occurs. At higher temperatures χ' increases again, following an S-shaped curve which is accompanied by a χ'' peak. Using a model two-level system for a thermally activated magnetic aftereffect process, $\tau=\tau_0\exp(Q/kT)$, the high-T χ' rise is explained by dynamic wall pinning and depinning owing to local directional ordering around domain walls with $Q\approx0.53$ eV and $\tau_0\approx1.7\times10^{-13}$ s. The low-T χ' peak is a consequence of domain-structure reconstruction and involves a long-range thermally hysteretic pseudostatic wall pinning and depinning process with average $Q\approx0.42$ eV and $\tau_0\approx10^{-10}$ s. The reasons for the anomalies in $\chi_{ac}(T)$ often found in rare-earth–transition-metal alloys are extensively discussed. [S0163-1829(96)07721-1]

I. INTRODUCTION

Magnetic properties of rare-earth–transition-metal based alloys have been an extensively studied subject owing to their possible large spontaneous magnetization M_s and magnetocrystalline anisotropy, which have brought some of them into practical applications as high-performance permanent magnets. Although their high-field dc properties are more important from the applications point of view, the low-field ac susceptibility ($\chi_{ac}=\chi'-j\chi''$) technique has recently been applied to such materials. This is because the anisotropy constants K_i ($i=1,2,3$) of these materials often show unusual temperature (4–300 K) dependence, and χ_{ac} can be a convenient probe of changes in K_i owing to direct relations between domain-magnetization-rotation (DMR) susceptibility, M_s, and K_i. K_i can even change sign at a certain temperature, causing a rotation of easy direction at a spin reorientation transition (SRT). Actually, the early motivation for applying the χ_{ac} technique to these materials was to probe SRT.[1,2]

However, there can also be a contribution to χ_{ac} from domain-wall displacements (DWD). When this contribution is not negligible, the situation becomes complicated, since factors other than M_s and K_i will play a role. Thus, different types of anomalous temperature dependence of χ_{ac} have been reported in the literature for these materials.[1–16]

χ_{ac} is considered anomalous when a relation to K_i cannot be found, even after classical technical magnetization theories for DWD susceptibility have been taken into account. In Ref. 3, having derived necessary formulas for susceptibilities owing to DMR and DWD, we analyzed the χ_{ac} data of a spherical $Nd_2Fe_{14}B$ single crystal, which has a conical to c-axis SRT at $\sim$130 K. We have found the following: (i) χ' at 8 A/m and 10 Hz or 80 A/m and 1 Hz measured along the c axis shows a sharp high peak at 127 K, where DMR susceptibility should be very close to zero and DWD susceptibility should change smoothly with T; and (ii) $\chi'(T)$ along the c axis shows a broad asymmetric peak between 100 and 230 K, which is unexpected since the effective K seems to change smoothly in the entire temperature range. Similar peaks or plateaus have also been observed in other materials, such as $Ho_2Fe_{14}B$, $Pr_2Fe_{14}B$, $Nd_2Fe_{14}C$, and $Nd_2Co_{14}B$.[1,4–6] (iii) In some materials, $Ho_2Fe_{14}BH_x$ and $Sm_2Fe_{17}H_x$, there exists a roughly symmetric $\chi'(T)$ peak around certain T.[7,8] (iv) In some alloys, Er_2Co_{17} and Tm_2Co_{17}, the anomaly is shown by a sharp rise in χ' accompanied by a χ'' peak.[9] (v) Many materials show an asymmetic $\chi'(T)$ peak followed by a rise in χ' and a χ'' peak.[9–15] An extensive review on this subject was recently made in Ref. 16, which concluded that the physical origin of the anomalies remained unclear, although various interpretations had been proposed in the literature.

We have discussed possible reasons for the type (i) anomaly.[3] Type (iii) is complicated since interstitial hydrogen atoms may take a part in the process. In this work, we choose to study a typical example of type (v), Sm_2Fe_{17}. The reasons are multiple: (1) There is a renewed interest in this material after a discovery that the addition of interstitial nitrogen could dramatically increase the Curie temperature and change the easy direction from the ab plane to the c axis, which is essential for high coercivity.[17] (2) Type (v) of anomaly is a more complete one than types (ii) and (iv); type (ii) may belong to type (v) if the temperature is extended above 300 K, while type (iv) can be regarded as type (v) when its first stage is absent. (3) There are more publications available for this material,[10,12,15] including a quantitative study on the time-varying nature of χ_{ac}.[8]

We have measured χ_{ac} under different conditions, and tried to obtain as much quantitative information as possible on domain-wall dynamics using phenomenological models. We will show that there are two distinct processes, dynamic domain-wall pinning and depinning and domain structure reconstruction with pseudostatic wall pinning and depinning,

that result in the type (v) anomaly. The analysis and discussion of the two processes provide some physical concepts and mathematical tools which will be useful for understanding of the various types of χ_{ac} anomaly.

II. EXPERIMENTAL

An ingot of Sm_2Fe_{17}, prepared by arc-melting and subsequent annealing at 1050 °C, was pulverized to a fine powder by ball milling for 15 min in cyclohexane. The powder was sieved to have particle sizes between 10 and 12 μm. The particles were roughly spherical. There was only a single phase as shown by the x-ray diffraction pattern, without any trace of α-Fe or other additional phases. The powder was mixed with epoxy in 1:8 mass ratio, formed into a cylinder, aligned in a magnetic field of 2 T during solidification, and then removed from the mold. Two samples of 3-mm diameter and 15-mm length were thus made with the easy directions of particles aligned along the length and diameter, respectively. X-ray data showed that the c axes (magnetically hard directions) of particles were perpendicular to the alignment direction and randomly distributed about it.

The real χ' and imaginary χ'' components of the complex ac susceptibility χ_{ac} were measured using a mutual impedance bridge. After cooling the sample from 300 K to $\sim$80 K in zero field, an ac field of amplitude $H_m = 113$ A/m was applied along the long axis of the sample. Three experiments were made for the longitudinally aligned sample as follows. (1) Temperature and frequency dependence: χ_{ac} at $f = 10$, 33.3, 111, 333, and 1000 Hz was measured periodically during warming with an averaged rate $dT/dt \approx 0.08$ K/min. (2) Warming-rate dependence: two runs of measurements were done with $dT/dt = 0.1$ and 1 K/min, respectively, and $f = 5$ and 111 Hz. (3) Time dependence: for each run, after cooling from 300 K to $\sim$80 K, T was quickly increased to a given value, 150, 155, 160, or 165 K, at which data for $f = 111$ Hz were taken in steps of 15 s or 30 s up to $\sim$900 min. Only the first experiment was repeated for the transversely aligned sample.

For calculating χ_{ac}, the sample volume was determined by the mass-density technique using the net mass and x-ray density of Sm_2Fe_{17} powder. No demagnetizing corrections were performed (the demagnetizing factor was about 0.07).

III. RESULTS

Since no pronounced anomaly has been detected for the transversely aligned sample, we give the results for the longitudinally aligned sample only. χ' and χ'', measured at $H_m = 113$ A/m and $f = 10$, 33.3, 111, 333, and 1000 Hz during warming with $dT/dt \approx 0.08$ K/min, as functions of temperature T are given in Figs. 1(a) and 1(b). We see that with increasing T from 87 K, χ' increases linearly up to 140 K, where a rounded maximum occurs. There is a rapid decrease in χ' between 150 and 160 K, after which it shows a broad minimum and rises again following an S-shaped curve. Corresponding to the two rises in χ', χ'' shows two peaks and falls to zero in between. Frequency dependence is found in the high-temperature S-shaped χ' segment and χ'' peak; they shift to higher T for higher f. All this agrees well with the data reported in Refs. 10, 12, and 15.

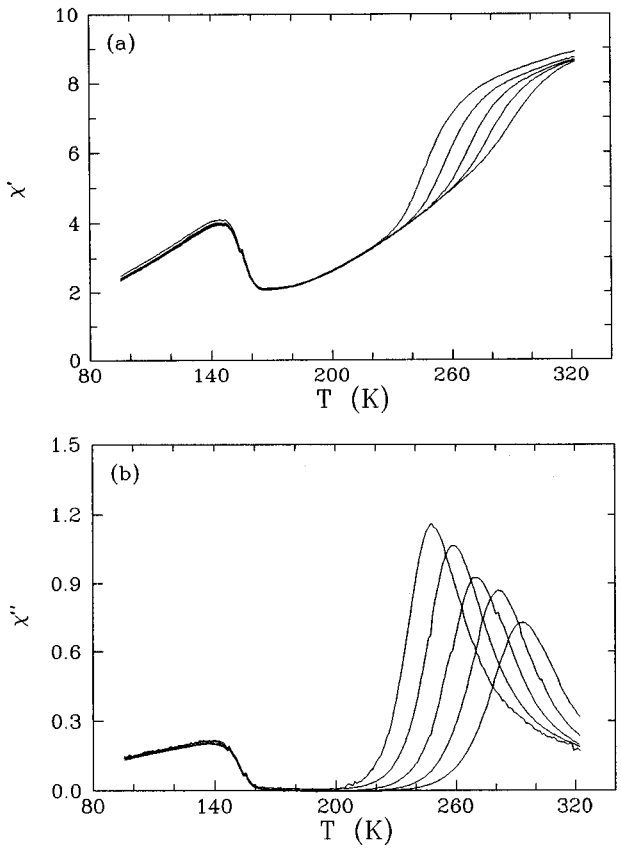

FIG. 1. χ' (a) and χ'' (b) as functions of temperature for $f = 10$, 33.3, 111, 333, and 1000 Hz measured during warming with an averaged rate of 0.08 K/min. f can be identified from the S-shaped $\chi'(T)$ and the $\chi''(T)$ peaks when $T > 200$ K; they shift to higher T at greater f.

Similar behavior is seen for other values of dT/dt. A comparison between $dT/dt = 0.1$ and 1 K/min is given in Figs. 2(a) and 2(b) for $f = 5$ Hz. We see that a tenfold increase in dT/dt extends the temperature range for the first rise in χ' and the first χ'' peak, but has less effect on the S-shaped χ' segment and the second χ'' peak.

In Fig. 3, we show the χ' decay with time t at constant T around the first χ' maximum. The decay at $T = 155$ K is much quicker than at $T = 150$ K. For higher T, the total change in χ_{ac} with t is small.

IV. MODELS

A. Time constant

To understand the above results concerning temperature, frequency, time, and warming-rate dependence of χ_{ac}, phenomenological models are necessary. For our sample of small particles at a maximum frequency of 1000 Hz, eddy-current damping is negligible. All time-varying phenomena should be due to structural relaxation, i.e., due to rearrangements of atoms. We use the popular model of a two-level system[18] for the thermal activation process, which results in a single time constant τ for the time-varying properties at a given temperature T.

The two-level model for the elementary relaxation events (such as atomic jumps and domain or domain-wall movements, see below) from the high- to low-energy level gives

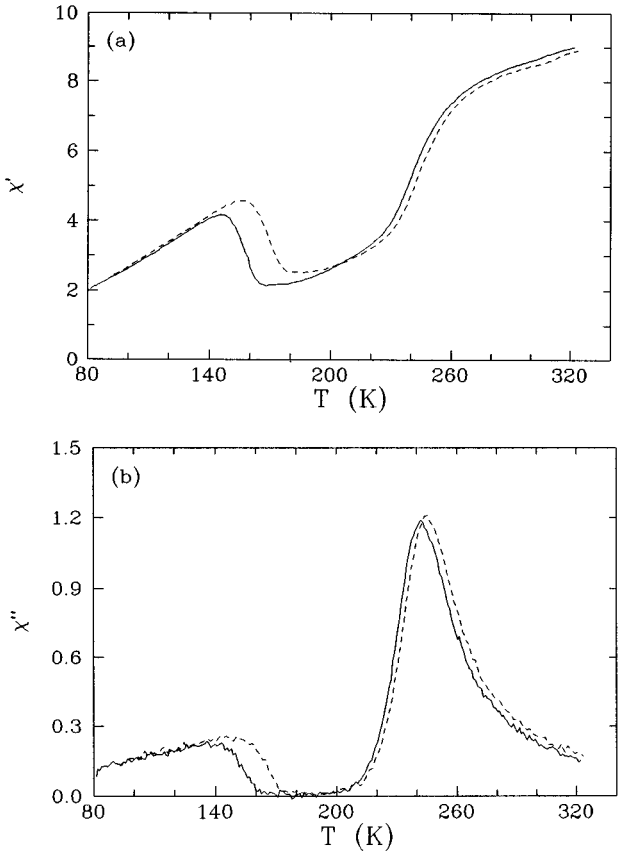

FIG. 2. χ' (a) and χ'' (b) as functions of temperature for $f=5$ Hz with warming rates of 0.1 (solid lines) and 1 K/s (dashed lines).

$$\tau=\tau_0\exp(Q/kT), \tag{1}$$

where Q is the activation energy, which is the energy barrier relative to the high level, k is the Boltzmann constant, and τ_0 is the preexponential factor.

B. Aftereffect of magnetization

At a fixed τ and if the time-varying properties are magnetization M and field H, the problem can be treated in terms of an equivalent circuit, in which constant inductance

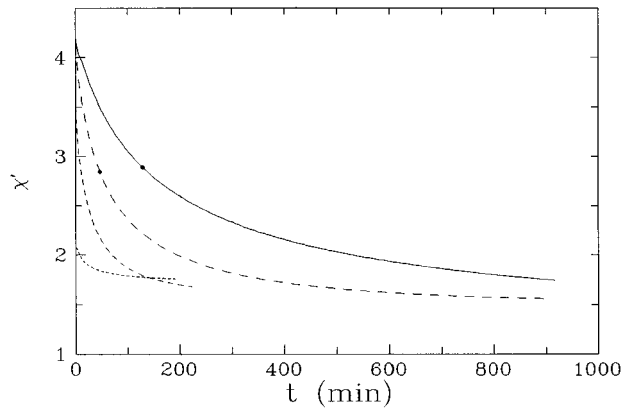

FIG. 3. Time dependence of χ' at $T=150$ (solid line), 155 (long dashed line), 160 (short dashed line), and 165 K (dotted line). Points on the first two lines indicate the time for half χ' decay at $T=150$ and 155 K.

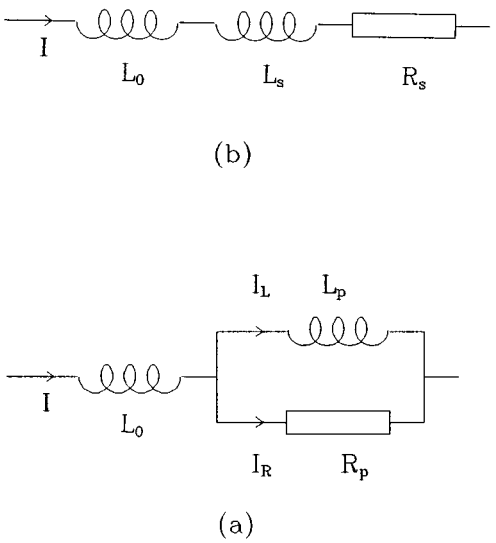

FIG. 4. Parallel (a) and serial (b) equivalent circuits of the sample.

L_p and resistance R_p are connected in parallel as shown in Fig. 4(a), like the case of classical eddy-current damping in its low-frequency limit.[19,20] The relation between L_p and M and H can be found by assuming a long sample (so that demagnetizing effects are negligible) of length l and cross-sectional area A, surrounded by an N-turn solenoid of the same length. Applying a dc current I to the solenoid, a field is produced by it as

$$H=NI/l. \tag{2}$$

In this case, L_p corresponding to the flux Φ_M produced by M of the sample is calculated as

$$L_p=\Phi_M/I=\mu_0N^2AM/lH=q\chi_{\rm dc}, \tag{3}$$

where $q=\mu_0N^2A/l$ and $\chi_{\rm dc}=M/H$ is the dc susceptibility. R_p is calculated from τ and L_p as

$$R_p=L_p/\tau. \tag{4}$$

For such a circuit, upon a stepwise I change from I_1 to I_2, the current I_L flowing through L_p will change from I_1 to I_2 exponentially with time constant τ. Equivalently, a sudden H change from H_1 to H_2 will result in an exponential M change from M_1 to M_2, because M is proportional to I_L:

$$M=\Phi_M/\mu_0NA=L_pI_L/\mu_0NA. \tag{5}$$

This is indeed the phenomenon of magnetization aftereffect.

In an ac field of amplitude H_m, using complex expressions, $M^*=M_me^{j(\omega t-\delta)}$ and $H^*=H_me^{j\omega t}$, for time-varying M and H, $\chi_{\rm ac}$ can be expressed as

$$\frac{1}{\chi_{\rm ac}}=\frac{H^*}{M^*}=\frac{1}{\chi_p'}+\frac{j}{\chi_p''}, \tag{6}$$

where two components of $\chi_{\rm ac}$ are defined from the equivalent circuit as

$$\chi_p'=L_p/q, \tag{7}$$

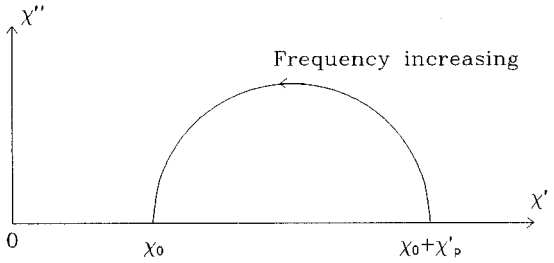

FIG. 5. Ideal χ'' versus χ' plot for χ_{ac} having a constant component χ_0 and frequency-varying components χ_s' and χ_s''.

$$\chi_p''=R_p/q\omega. \tag{8}$$

Simple impedance calculations lead to another pair of component susceptibilities for an equivalent circuit of series connected L_s and R_s [Fig. 4(b)], defined by

$$\chi_{ac}=\chi_s'-j\chi_s''=L_s/q-jR_s/q\omega. \tag{9}$$

These two pairs of component susceptibilities have the following relations:

$$\chi_s'=\chi_p'[1+(\chi_p'/\chi_p'')^2]^{-1}=\chi_p'[1+(\omega\tau)^2]^{-1}, \tag{10}$$

$$\chi_s''=\chi_p''[1+(\chi_p''/\chi_p')^2]^{-1}=\chi_p'[\omega\tau+(\omega\tau)^{-1}]^{-1}. \tag{11}$$

From Eqs. (10) and (11) we see that although $\chi_p'=\chi_{dc}$ does not change, both χ_s' and χ_s'' change simultaneously with frequency $f=\omega/2\pi$. Changing ω from 0 to ∞, χ_s'' as a function of χ_s' is a semicircle. In the literature, the low- and high-f limits are often called the isothermal and adiabatic susceptibilities.[21] If there is a frequency-independent nonzero real component χ_0 in the actual χ_{ac}, then an inductance L_0 should be connected to the above equivalent circuits, as shown in Figs. 4(a) and 4(b), and χ'' as a function of χ' is shown in Fig. 5.

C. Aftereffect of χ_{ac}

In the above model, increasing $\omega\tau$ from 0 to ∞ makes χ' decrease from $\chi_0+\chi_p'$ to χ_0, and makes χ'' increase from 0 to $\chi_p'/2$ and then decrease to 0. We can study the observed frequency dependence based on this model.

If $\omega\tau\gg1$, we should always have $\chi_{ac}=\chi_0$. This is in contradiction to our results for the time and warming-rate dependence. Therefore, another model is necessary for the aftereffect of χ_{ac} itself. In this model, the behavior of χ_0 will be the same as that of M described in the model of the magnetization aftereffect. The physical meaning of these two aftereffects will be described in Secs. VI B and VI C.

V. DATA ANALYSIS

A. Temperature and frequency dependence

According to Eq. (1), τ is constant at a given T. Since the T- and f-dependence measurements were made in the same run with periodically changing f, different f at a given T corresponds to the same process. Thus, it should be possible to treat χ'' vs χ' data using Eqs. (10) and (11) for each value of T. Actually, the treatment can be made for T between 240 and 280 K only, where χ'' increases remarkably with decreasing f. The χ'' vs χ' functions for $T=240$, 250, 260, 270, and 280 K obtained from the data given in Figs. 1(a) and 1(b) are plotted in Fig. 6(a). We can see that not less than three data points on the high-f side always fit on a semicircle, consistent with the model of a constant τ at each value of T.

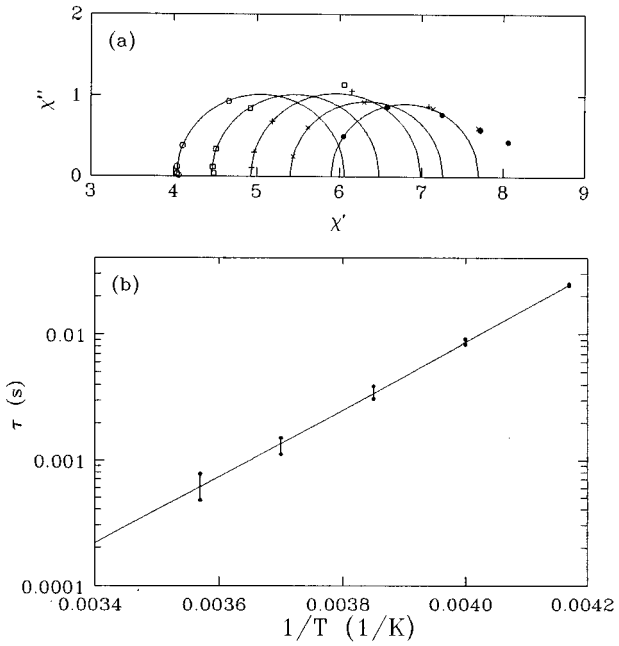

FIG. 6. (a) Semicircular data fits for $T=240$ (○), 250 (□), 260 (+), 270 (×), and 280 K (●). (b) τ versus $1/T$ obtained from (a).

We further calculate τ from each pair of χ' and χ'', written as τ' and τ'', that is located on the fitting semicircle using

$$\tau'=\sqrt{\chi_p'/\chi_s'-1}/2\pi f, \tag{12}$$

$$\tau''=[\chi_p'/\chi_s''+\sqrt{(\chi_p'/\chi_s'')^2-4}]/4\pi f, \tag{13}$$

derived from Eqs. (10) and (11). In these equations,

$$\chi_s''=\chi'', \tag{14}$$

$$\chi_s'=\chi'-\chi_0. \tag{15}$$

τ' and τ'' for different values of T and f, calculated from Eqs. (12)–(15) using the measured χ' and χ'' in Figs. 1(a) and 1(b) and the fitting parameters χ_0 and χ_p', are listed in Table I. We see that most pairs of τ' and τ'' are in a good agreement and their average has a weak frequency depen-

TABLE I. τ',τ'' (ms) for different values of T and f.

τ',τ''	10 Hz	33.3 Hz	111 Hz	333 Hz	1000 Hz
240 K	23.9, 24.3	24.4, 24.7	28.9, 24.2		
250 K		8.77, 8.90	8.59, 8.42	5.54, 8.34	
260 K			3.77, 3.80	3.64, 3.24	2.28, 3.08
270 K			1.49, 1.53	1.32, 1.29	1.13, 1.18
280 K			0.83, 2.56	0.61, 0.64	0.53, 0.53

dence at each temperature. Therefore, the model of magnetization aftereffect is satisfactory for a major part of the f dependence.

Applying a standard data treatment, we obtain an average τ for each value of T with a standard error. The resulting τ vs $1/T$ function is shown in Fig. 6(b). A linear fit according to Eq. (1) gives $\tau_0 = 1.7\times 10^{-13\mp 0.6}$ s and $Q = 0.53 \pm 0.03$ eV. Note that the orders of signs for both errors are opposite since they are actually correlated.

B. Time dependence

We see from Fig. 6(a) that not all five frequency points for the same T can be fitted by the same semicircle, which means that the simple model can only partially account for the data. Similarly, the results for time dependence given in Fig. 3 are not exponential, so that the model of χ_{ac} aftereffect is only approximately valid too. In order to have an estimate for τ_0 and Q, we use the time when χ' changes as half of the total change to represent τ. Since the χ' vs t curve at $T = 155$ K is more complete, we use it to obtain the half χ' change, and assume it to be the same for $T = 150$ K. This gives $T_1 = 150$ K, $\tau_1 = 7740$ s and $T_2 = 155$ K, $\tau_2 = 2820$ s. They are substituted in Eq. (1):

$$\tau_{1,2} = \tau_0 \exp(Q/kT_{1,2}), \tag{16}$$

whose solutions are

$$Q = k \ln \frac{\tau_1}{\tau_2}\left(\frac{1}{T_1} - \frac{1}{T_2}\right) = 0.40 \text{ eV}, \tag{17}$$

$$\tau_0 = \tau_1 \exp(-Q/kT_1) = 2.9\times 10^{-10} \text{ s}. \tag{18}$$

C. Warming-rate dependence

To obtain τ_0 and Q from the warming-rate dependence is more complicated, since both T and t change simultaneously. The procedure we have applied is as follows. An averaged Q is obtained as

$$Q = k \ln 10/(1/T_1 - 1/T_2) = 0.45 \text{ eV}, \tag{19}$$

where $T_1 = 157.2$ K and $T_2 = 168.8$ K, being the temperatures for the half change of χ' at $dT/dt = 0.1$ K/min and 1 K/min, respectively. This equation is obtained from Eq. (1) considering $\tau_1/\tau_2 = 10$, which is a direct consequence of the 10-time difference between both dT/dt's. Similar calculations made for the χ' maximum and minimum lead to $Q = 0.48$ and 0.42 eV, respectively. Thus, we have $Q = 0.45 \pm 0.03$ eV for the entire process.

With these values of Q, we apply Eq. (1) again for $dT/dt = 0.1$ K/min and the average temperatures (as T) and times (as τ) for the first and second halves of χ' change. This gives $\tau_0 = 2.2\times 10^{-12}$ s and 2.9×10^{-10} s for the first and second halves. Thus, the averaged $\tau_0 = 2.5\times 10^{-11\mp 1.1}$ s.

VI. DISCUSSION

A. Activation energy and preexponential factor

The data analysis in Sec. V gives three pairs of Q and τ_0, 0.53 eV and 1.7×10^{-13} s, 0.40 eV and 2.9×10^{-10} s, and 0.45 eV and 2.5×10^{-11} s, for the temperature-and-frequency, time, and warming-rate dependences. From them we see a general rule that a smaller Q corresponds to a greater τ_0.

It is well known that $\tau_0 \sim 10^{-13}$ s is characteristic of a Debye process. Therefore, the χ_{ac} change with f should be related to thermally activated individual atomic jumps of very short range; an elementary process is accomplished by one or few atomic jumps. For the other two changes in χ_{ac}, τ_0 is two or three orders of magnitude greater. This implies that an elementary process is related to a series of many successive atomic jumps, i.e., involves a long-range atomic movement.

If a process has to be accomplished in one atomic jump, Q should be greater since it has no opportunities to choose an easy way. On the other hand, if there is a long way to go from the starting to ending point, each atom can easily choose an easy direction to jump, so that the averaged Q is lower. The rule mentioned above has thus been justified.

B. Directional ordering

In the phenomenological model described in Sec. IV B, we have assumed a magnetization aftereffect with a single time constant τ. Having estimated the τ_0 and Q relevant for the temperature and frequency dependence, we can now discuss its physical basis. The aftereffect of M upon a sudden change in H is a classical phenomenon in ferromagnetic materials.[22] The effect occurring here should be the Richter aftereffect with a relatively narrow and strongly temperature-dependent τ spectrum.

The mechanism of such an aftereffect was studied 40 years ago for substitutive and interstitial solid solutions.[23–26] In general, there is a thermally activated directional ordering of like-atom pairs or interstitial atoms with respect to the lattice. This ordering is induced by spontaneous magnetization $\mathbf{M_s}$ at relatively high T, accompanied by an induced uniaxial anisotropy with easy axis along $\mathbf{M_s}$. In the time scales of usual experiments, the like-atom pair ordering often occurs at $T > 700$ K, resulting at zero field in a Perminvar magnetization behavior, which is characterized by a high-field wasp-waist hysteresis loop and an extended low-field linear initial curve, after cooling, while the interstitial atom ordering can occur even below room temperature. The concept of directional ordering was developed in the study of amorphous alloys, where intrinsic chemical and geometrical short-range ordering exists within clusters accompanied by a local uniaxial anisotropy. Owing to the richness of free volumes, the easy axes of the clusters are easier to align, so that the aftereffect becomes more pronounced, occurring at lower T.[27–30] In the present material with a complicated rhombohedral structure, in which many stoichiometric vacancies exist,[8] smaller Fe atoms are easy to move through the vacancies, so that the directional ordering can occur below room temperature.

It is well known that the domain wall is a region across which spins (elementary magnetic moments) change directions gradually owing to a compromise between magnetocrystalline anisotropy energy and exchange energy. The easy direction of the developed local induced anisotropy within a static wall in zero field coincides with the direction of the spin, and this results in an extra potential superimposed on

the initial pinning potential well resulting from other fixed sources, or an extra pinning force against the wall movements from its equilibrium position. Thus, if applying a small field from time to time during directional ordering to measure susceptibility, one will see the susceptibility decrease with time elapsing owing to the development of extra pinning. This is a kind of magnetic aftereffect, namely susceptibility disaccommodation.

C. Dynamic wall pinning and depinning

In comparison with the case of zero field, the directional ordering in a small ac field is different. Since the domain wall vibrates within a pinning potential well, the directions of spins within a certain distance greater than the wall thickness are changing periodically with time. If $\omega \gg 1/\tau$, τ being the time constant for directional ordering, then the atomic jump cannot follow the instant direction of the spin, and instead, it tends to jump according to the time-averaged direction of the spin, resulting in a shallower and wider extra pseudostatic potential well, which has the same bottom as the initial potential well, and gives rise to a weaker extra pinning compared to the case of zero field. Like the zero-field case, such a wall pinning develops with time t, and reaches its maximum when $t \gg \tau$.

We now inspect the frequency dependence at a fixed τ, assuming the measuring time at each frequency to be much greater than τ. At all values of frequency, there is a fixed common initial pinning potential not due to directional ordering, and the frequency dependence results from the extra potential well of directional ordering. If $\omega \ll 1/\tau$, the local directional ordering can be fully developed in each spin configuration. Thus, the bottom of the extra well will always coincide with the wall center during wall movements, and no extra pinning force is exerted on the wall. On the other hand, if $\omega \gg 1/\tau$, the extra potential well is pseudostatic as described above with the same bottom as the initial well. Therefore, the extra pinning force takes its maximum value.

Complicated situations occur when $\omega\tau$ is not very far from unity. In this case, the local directional ordering can neither catch up with the wall movement as when $\omega \ll 1/\tau$ nor tend to point in the time-averaged spin configuration as when $\omega \gg 1/\tau$, and the easy directions of the local induced anisotropies always lag behind the instant spin directions. In other words, there is a position delay of the moving extra potential well to the moving wall.

Investigating the process more closely, we will find that the wall velocity during ac magnetization is not constant, and it takes a maximum value when the wall passes the equilibrium central position and is zero when the wall reaches the two extremes. These facts will justify the choice of the parallel equivalent circuit given in Sec. IV B.

The simplest equivalent circuit should be a connection of an inductance and a resistance, both of which express the effect of wall displacement and its retardation by the delayed pinning well, respectively. We argue that a parallel connection of L_p and R_p satisfies the physical requirements. Because the wall velocity is zero when it reaches the extremes (at positive and negative maximum M), the extra well can follow the wall so that no extra pinning force is exerted on the wall at any frequency. This requires the current flowing through the resistance $I_R = 0$, and the situation is just like this; since L_p and R_p are parallel, and the voltage U across R_p is the same as that across L_p, which is zero since $U \propto dI_L/dt = dM/dt = 0$. The maximum retardation occurs when the wall passes its central position with a maximum velocity and $M = 0$. This is also consistent with the parallel equivalent circuit, since at this moment, we have $I_R = I$ and the whole applied field H is used to balance the maximum pinning force. The validity of the parallel equivalent circuit leads to the validity of all the equations in Sec. IV B.

The parallel equivalent circuit is not valid if the measuring time at each frequency is not much greater than τ. However, we can have a simple case when $\omega\tau \gg 1$. Although this circuit is not valid in this case, we still have $\chi'' = 0$ because there is no retardation for the wall resulting from a pseudostatic extra potential well at such a high frequency. Thus, with developing the directional ordering, $\chi_{ac} = \chi'$ can be used to probe the strength of induced anisotropy at each instant, which is somewhat lower than that of the zero-field case as explained in Sec. VI B. This is the physical basis of the model of the χ_{ac} aftereffect.

Actually, the single-τ model of χ_{ac} aftereffect is approximate. A better approximation should be the $1/\chi_{ac}$ aftereffect as studied in Ref. 8, since the directional ordering results in an induced anisotropy which is proportional to $1/\chi_{ac}$. If the time-varying part is small compared with the fixed part of susceptibility, the two aftereffects will give similar results.

In summary, owing to local directional ordering with time constant τ and resultant local induced anisotropy, the moving wall in the ac case is subjected to an extra pinning force resulting from an extra potential well. If the measuring time is much greater than τ and when $\omega \ll 1/\tau$, the well can catch up with the wall movements so that no extra pinning force is exerted on the wall. When $\omega \ll 1/\tau$, the well is pseudostatic so that a maximum extra pinning force will act on the wall. In all the intermediate cases, there is an extra pinning force retarding the wall movements. Its effect can be expressed by the parallel equivalent circuit, with $\chi'' = 0$ in the above two limits. These situations altering with $\omega\tau$ are referred to as the dynamic wall pinning and depinning. If the measuring time is much less than τ and $\omega \gg 1/\tau$, then the wall is always in a pseudostatically pinned state, and $\chi_{ac} = \chi'$ can be a quantity to probe the process of directional ordering.

D. Temperature and frequency dependence

With the above ideas of dynamic wall pinning and depinning, the observed temperature and frequency dependence can be explained as follows. It is directly related to DWD at low ac field when domain walls vibrate within their pinning potential wells. It is related to elementary processes of single atomic jumps, so that $\tau_0 \sim 10^{-13}$ s. Increasing T will decrease τ quickly according to Eq. (1). Therefore, the frequency-dependent χ'' and χ' occur in a certain temperature range, where $\omega\tau$ is comparable with 1. At any given f value, we have $\omega\tau \gg 1$ at low T, so that the walls are tightly pseudostatically pinned having a low χ' and zero χ''. With increasing T, $\omega\tau$ decreases to values not far from 1, the dynamic depinning occurs, so that χ' increases and $\chi''(T)$ presents a peak. A higher f will delay the decrease of $\omega\tau$ with respect to T, so that the χ' rise and χ'' peak shift to

higher T at higher f. With directional ordering, such an anomalous temperature and frequency dependence has been observed in all the rare-earth–transition-metal alloys that show anomalies of types (iv) and (v).

E. Domain structure reconstruction

Since $\omega\tau$ is always much greater than 1 at lower T in the experiments at audio frequency, χ' should decrease continuously (though very slowly) with decreasing T owing to the χ_{ac} aftereffect. So why does χ' increase to a maximum at $T\sim 150$ K? We believe this to be caused by a domain structure reconstruction (DSR).

The main reason for domain structure to exist in a ferromagnetic body is to minimize magnetostatic energy. A compromise between the wall energy and magnetostatic energy determines the actual domain structure. The wall energy density γ_B is proportional to $\sqrt{K_{\text{eff}}}$, where K_{eff} is the effective magnetocrystalline anisotropy constant. Since Sm_2Fe_{17} has a rhombohedral structure with an easy ab plane, the domain wall will preferably lie parallel to this plane so that K_{eff} and γ_B can be smaller. Using

$$E_k = K_1\sin^2\theta + K_2\sin^4\theta + K_3\sin^4\theta\,\cos 6\phi \qquad (20)$$

for the anisotropy energy, K_{eff} should be proportional to K_3. Thus, if K_3 changes rapidly at $T\sim 150$ K, γ_B will change accordingly. An increase (or decrease) of γ_B requires a decrease (or increase) of the total wall area, and thus a smaller (or greater) number of walls to compromise the static energy. Therefore, some walls will tend to move out of (or into) the particles even without H applied.

Since no data on $K_3(T)$ are available for the present material, we assume reasonably that K_3 increases rapidly with decreasing T through 150 K. With this assumption, the anomaly can be explained as follows. With decreasing T to ~ 150 K, the walls are pseudostatically pinned tightly, as explained in Sec. VI C. A small K_3 change is not enough to depin them, and only when a sharp increase in K_3 occurs at ~ 150 K so that the total wall energy increases to values enough to overcome the effects of pinning potentials, will a DSR take place. The depinned walls are easy to move since pseudostatic wall pinning to the new walls develops very slowly owing to a great τ at decreased T, and this corresponds to a rise in χ' during cooling in spite of the decreased wall number. When the sample is warmed again, another DSR occurs accompanied by pseudostatic wall pinning with τ comparable to the experimental time, so that χ' decreases. Thus, the DSR and pseudostatic wall pinning and depinning explain the general feature of the T dependence of χ'.

We can find two examples from the literature to support the above idea of DSR. In Ref. 3 for a $Nd_2Fe_{14}B$ single crystal with an easy c axis, the anomalous χ' rise with decreasing T occurs at 230 K, and one can see a rapid increase in $K_{\text{eff}}=K_1+K_2-|K_3|$ from constant 6.4 MJ/m^3 above 250 K to 7.8 and 9.0 MJ/m^3 at 215 and 175 K, respectively. Such a K_{eff} increase could force the pinned wall to depin so that a DSR takes place at 230 K. In Ref. 9 for Dy_2Co_{17} samples with an easy basal plane, the crystalline anisotropy on the easy plane disappears ($K_3\rightarrow 0$) at ~ 160 K with warming. In accordance with this, there is a very sharp χ' drop at the same T, and this can only be explained by a sudden DSR owing to a sudden change in K_{eff} ($\propto K_3$), since the behavior is against the classical theory of technical magnetization, which would predict a sudden rise in χ' opposite to the observed anomaly.

F. Thermally hysteretic wall pinning and depinning

As mentioned in Sec. VI A, τ_0's derived from the time and warming-rate dependences of the low-temperature anomaly are different and are 10^2–10^3 times greater than that derived from the frequency dependence of the high-temperature anomaly. This indicates a complicated process occurring at ~ 150 K.

The high-T process is simpler since domain walls are vibrating but not traveling. The local directional ordering requires one or few atomic jumps to change the orientation of Fe-atom pairs. The process is thermally reversible also, since the wall movements are within a potential well of fixed position.

The low-T process is different. To understand the difference we have to describe the DSR process in more detail as follows. The decrease in the wall number occurs when the domain sizes increase and the walls move outwards from the particle center. The outmost domains and walls are disappearing successively during the process. On the other hand, the increase in the wall number involves inwards wall movements and the creation of new domains and walls on the particle surface. Both processes are irreversible since during the long range wall movements and domain creations potential barriers of wall pinning and domain nucleation must be overcome. Thus, DSR's during cooling or warming cannot occur at the same temperature where K_3 shows a rapid change, i.e., the DSR is thermally hysteretic; DSR during cooling should occur at lower T because of the impedance of extra pinning potential wells upon the moving walls, whereas DSR during warming should occur at higher T owing to the domain nucleation barriers. In fact, a 2–4 K difference for the low-T anomaly has been found for the longitudinally aligned sample between warming and cooling. Such a T difference was also reported for $Nd_2Fe_{14}B$.[6,16]

Actually, the elementary events in this case are not easy to define. For the irreversible wall movements and domain nucleations, they should be the movements of the wall or domain as a whole, but considering the directional ordering, which occurs during the DSR, they should be the atomic jumps. Incorporating both together, we can explain the large τ_0 as follows. During the DSR, the walls must move for a rather large distance. If the average distance is as large as 1 μm, which is more than 10^3 atomic distances, then a 10^3 times greater τ_0 than the Debye process is possible.

The big difference in τ_0 between the time and rate dependences may be related to the difference in starting and ending states of different runs of experiments, since the cooling rates were not controlled and they should be an important factor in the thermally hysteretic process. The difference can also be understood in a similar way to that described in Sec. VI A. In the time dependence experiments, the ending state for each T is fixed and the relaxation develops for a long time, so that the atoms can find easier directions to jump and this corresponds to a smaller Q and greater τ_0 than those in the rate

dependence experiments, where the target state for the relaxation is changing with time since K_3 is a function of T and the atoms have to adjust the jump directions accordingly and reach the final state in a short period. Owing to this complexity, we take the average results obtained from two experiments for the pseudostatic wall pinning and depinning process, i.e., $Q \approx 0.42$ eV and $\tau_0 \approx 10^{-10}$ s.

G. Other influencing factors

The dynamic (or pseudostatic) and thermally hysteretic wall pinning and depinning together with DSR have explained the essential part of our experimental data. There are some other phenomena that are worth commenting on.

As shown in Figs. 1 and 2 at lower temperatures, a $\chi''(T)$ peak accompanies a $\chi'(T)$ peak without frequency dependence. This is in contrast with those at high temperatures, where a $\chi''(T)$ peak accompanies a χ' rise with a strong frequency dependence. The low-T nonzero χ'' should be ascribed to magnetic hysteresis effect. The reason why $\chi''=0$ at higher T is that the walls are tightly pinned by local induced anisotropy, and they can only vibrate reversibly within the pinning well at $H_m = 113$ A/m. When T is lower, some walls that have been pinned by local induced anisotropy move to new positions after DSR become depinned at the same H_m, since local anisotropies corresponding to the new domain structure do not have enough time to induce. As a result, irreversible wall movements take place and $\chi'' > 0$. If this is true, χ'' in low-T region should be able to be reduced by decreasing H_m.

In the above, we did not discuss other sources of pinning besides local induced anisotropy. Sources like inclusions, stresses, and particle boundaries generally exist, and if their effect on domain mobility is dominant then the anomaly owing to the reasons we have discussed will be negligible. Moreover, the strength of those effects is always proportional to γ_B or $\sqrt{K_{\text{eff}}}$, and therefore, the anomaly should mainly occur in a T region with smaller K_{eff}.

Studying the anomalies, the authors of Refs. 6 and 16 reported a very interesting annealing effect: some samples did not show an anomaly in the as-prepared state, but the anomaly was induced by annealing. This annealing effect can be partially attributed to the reduction of other pinning effects. If the annealing does not remove the stochiometric vacancies, then an enhanced anomaly will be observed. However, if it removes the vacancies, there would be an opposite annealing effect, i.e., it eliminates the anomaly. Actually, some samples were prepared using our powder after evacuating at 350 °C for 50 min, and the results showed a disappearance of the anomaly.

Recently, the effect of hydrogen content on χ_{ac} of this material has been studied in detail.[31] It seems more logical that the vacancy movements are through hydrogen atoms rather than iron atoms; the former are much smaller and easy to jump around at low temperatures. If so, the annealing effect can be attributed to the reduction of hydrogen content.

H. Further remarks

Here we have studied a typical rare-earth–transition-metal alloy and tried to describe concepts and mathematics relevant to an understanding of the ac susceptibility. Our main efforts have been put on the applications of existing knowledge to experimental phenomena, although the concept of DSR may be new.

We find that a commonly accepted idea that a SRT is not the origin of the χ_{ac} anomalies dealt with in this paper since they are not related to the sign change in K_1. Moreover, two previous works are relevant to the understanding of the anomalies. Sartorelli and Kronmüller[8] studied the $1/\chi_{\text{ac}}$ aftereffect for the same material in a certain T range and found that the maximum effect occurred near the temperature where the low-T anomaly was observed. They therefore connected the low-T anomaly to this aftereffect which is related to the relaxation of stoichiometric vacancies. Kou *et al.*[9] compared the measured $\chi_{\text{ac}}(T)$ and high-field $M(T)$ curves of polycrystalline and monocrystalline Dy_2Co_{17} samples. They found that the χ_{ac} minimum was at $T \approx 160$ K where the basal plane anisotropy disappeared ($K_3 \rightarrow 0$) with increasing T. Thus, they connected the anomaly to the intrinsic parameter K_3 based on classical technical magnetization theories.

Our explanations are a development of these two interpretations. In our opinion, the $1/\chi_{\text{ac}}$ aftereffect at lower T studied in Ref. 8 reflects the physics in the high-T χ_{ac} anomaly, so that the values $\tau_0 \approx 3.6 \times 10^{-13}$ s and $Q \approx 0.50$ eV they obtained are very close to those determined from our frequency dependence data at higher T. This is because their experiments were performed on ac demagnetized samples so that DSR took place artificially before each measurement. After the DSR, the walls are pinned around fixed positions without traveling, and the atomic process is the same as that actually occur at high T without DSR, i.e., the local directional ordering. Therefore, if one can study directly the wall dynamics by the frequency dependence at higher T, its mechanism can also be studied by the χ_{ac} (or $1/\chi_{\text{ac}}$) aftereffect at lower T.

In contrast with the explanation given in Ref. 9, we have attributed the low-T anomaly to both a postulated K_3 change and a magnetic aftereffect. As already explained in Sec. VI E, the observed K_3 change in Dy_2Co_{17} will result in a change in χ_{ac} opposite to that at the observed (low-T) anomaly if classical theories are used; only when both the DSR and magnetic aftereffect are considered, can the observed anomaly be explained.

It is interesting to look for the $\chi'(T)$ curve that corresponds to the case without an anomaly. Since according to the above ideas the anomaly will disappear if there is no magnetic aftereffect, this normal $\chi'(T)$ should be one whose low-T and high-T portions coincide with the low-f curve in Fig. 1(a) and whose middle part is an interpolation of both between 140 and 280 K. This curve should also have small thermal hysteresis owing to many small DSR's with changing T.

It is also interesting to compare DSR with SRT. The latter is mainly related to the sign change in K_1 and results in a thermally reversible bending point in the DMR susceptibility vs T curve. The former is related to a rapid change in K_{eff} (K_3 for materials with an easy plane) and results in a thermally hysteretic DWD susceptibility decrease with increasing T.

Incorporating DSR, SRT with magnetic aftereffects and the effect occurring at $K_1=0$ studied in Ref. 3 (a special kind of field induced DSR), most phenomena observed in rare-earth–transition-metal alloys can be basically understood. However, there are still problems that need to be studied further. These include, for example, how one can define the elementary events in DSR and study more properly the relaxation process, what the origin is of the anomaly of type (iii) in the compounds with hydrogen, and why a warming rate dependence is also shown in the high-T region (see Fig. 2).

VII. CONCLUSION

We have measured the complex ac susceptibility of an aligned sample of Sm_2Fe_{17} powder in the temperature range where anomalous behavior occurs. The anomalous rise in χ' accompanied by a χ'' peak at $T>200$ K is explained by dynamic domain-wall pinning and depinning, which is a consequence of thermally activated local directional ordering of Fe atoms. This process has a very short range, with $Q\approx 0.53$ eV and $\tau_0\approx 1.7\times 10^{-13}$ s. A separate χ' peak around 150 K is ascribed to domain structure reconstruction which is related to a change in the in-plane magnetocrystalline anisotropy K_3 and thermally hysteretic pseudostatic wall pinning and depinning. This is a long range process with $Q\approx 0.42$ eV and $\tau_0\approx 10^{-10}$ s. Anomalies of χ_{ac} in many rare-earth–transition-metal alloys have been explained either by intrinsic properties or by extrinsic defects alone. Our work on the typical example of Sm_2Fe_{17} shows anomalies which are intimately related to both the intrinsic crystalline anisotropy constants and the extrinsic defect structure.

ACKNOWLEDGMENTS

We are grateful to Stephen Brennan for help with some of the measurements and to L. M. Martinez for his help in experiments. The research was partially supported by the European Brite/Euran Program.

*Permanent address: Faculty of Physics, University of Sofia, 1126 Sofia, Bulgaria.

[1] R. Grössinger, X. K. Sun, R. Eibler, K. H. J. Buschow, and H. R. Kirchmayr, J. Magn. Magn. Mater. **58**, 55 (1986).
[2] P. A. Algarabel, A. Del Moral, M. R. Ibarra, and J. I. Arnaudas, J. Phys. Chem. Solids **49**, 213 (1988).
[3] D.-X. Chen, V. Skumryev, and H. Kronmüller, Phys. Rev. B **46**, 3496 (1992).
[4] X. C. Kou and R. Grössinger, J. Magn. Magn. Mater. **95**, 184 (1991).
[5] X. C. Kou, C. Christides, R. Grössinger, H. R. Kirchmayr, and A. Kosticas, J. Magn. Magn. Mater. **104-107**, 1341 (1992).
[6] J. Bartolomé, L. M. García, F. J. Lázaro, Y. Grincourt, L. G. de la Fuente, C. de Francisco, J. M. Muñoz, and D. Fruchart, IEEE Trans. Magn. **30**, 577 (1994).
[7] F. J. Lázaro, L. M. García, J. Bartolomé, D. Fruchart, and S. Miraglia, J. Magn. Magn. Mater. **114**, 261 (1992).
[8] M. L. Sartorelli and H. Kronmüller, in *Proceedings of the 8th International Symposium on Magnetic Anisotropy and Coercivity in RE-TM Alloys*, edited by C. A. F. Manwaring, D. G. R. Jones, A. J. Williams, and I. R. Harris (University of Birmingham, Birmingham, 1994), p. 53.
[9] X. C. Kou, T. S. Zhao, R. Grössinger, and F. R. de Boer, Phys. Rev. B **46**, 6225 (1992).
[10] R. Grössinger, X. C. Kou, T. H. Jacobs, and K. H. J. Buschow, J. Appl. Phys. **69**, 5596 (1991).
[11] X. C. Kou and R. Grössinger, J. Magn. Magn. Mater. **104-107**, 1339 (1992).
[12] O. Isnard, C. Kolbeck, S. Miraglia, J. L. Soubeyroux, D. Fruchart, E. Tomey, C. Rillo, and M. Guillot, J. Magn. Magn. Mater. **104-107**, 2003 (1992).
[13] X. C. Kou, T. S. Zhao, R. Grössinger, H. R. Kirchmayr, X. Li, and F. R. de Boer, Phys. Rev. B **47**, 3231 (1993).
[14] Z. G. Zhao, J. Y. Wang, Y. P. Ge, F. M. Yang, X. K. Sun, Y. C. Chuang, K. H. J. Buschow, and F. R. de Boer, J. Appl. Phys. **73**, 5875 (1993).
[15] M. L. Sartorelli, L. Kleinschroth, and H. Kronmüller, J. Magn. Magn. Mater. **140-144**, 997 (1995).
[16] L. M. García, Doctoral thesis, Universidad de Zaragoza, 50009 Zaragoza, Spain, 1994.
[17] J. M. D. Coey and H. Sun, J. Magn. Magn. Mater. **87**, L251 (1990).
[18] C. Y. Huang, J. Magn. Magn. Mater. **51**, 1 (1985).
[19] D.-X. Chen, *Physical Bases of Magnetic Measurements* (China Mechanical Industry, Beijing, 1985), p. 155.
[20] D.-X. Chen, *Ballistic and Bridge Methods of Magnetic Measurements of Materials* (China Metrology, Beijing, 1990), p. 47.
[21] A. J. van Duyneveldt, J. Appl. Phys. **53**, 8006 (1982).
[22] R. M. Bozorth, *Ferromagnetism* (D. Van Nostrand, New York, 1956), p. 788.
[23] L. Néel, Comp. Rend. **237**, 1613 (1953).
[24] L. Néel, J. Phys. Radium **15**, 225 (1954).
[25] S. Taniguchi and M. Yamamoto, Sci. Rep. Res. Inst. Tohoku Univ. **A6**, 330 (1954).
[26] S. Taniguchi, Sci. Rep. Res. Inst. Tohoku Univ. **A8**, 173 (1956).
[27] T. Egami, in *Amorphous Metallic Alloys*, edited by F. E. Luborsky (Butterworths, London, 1983), p. 100.
[28] H. Fujimori, in *Amorphous Metallic Alloys* (Ref. 27), p. 300.
[29] D.-X. Chen, C. F. Conde, H. Miranda, and A. Conde, J. Magn. Magn. Mater. **111**, 135 (1992).
[30] D.-X. Chen, M. Vázquez, and C. de Julian, J. Magn. Magn. Mater. **115**, 295 (1992).
[31] M. L. Sartorelli, Doctoral thesis, Max-Planck-Institute für Metallforschung, Institute für Physik, Stuttgart, Germany, 1995.